Deciphering a structural signature of glass dynamics by machine learning

Han Liu [1,*] Morten M. Smedskjaer,[2] and Mathieu Bauchy [3]

[1]*SOlids inFormaTics AI-Laboratory (SOFT-AI-Lab), College of Polymer Science and Engineering,
Sichuan University, Chengdu 610065, China*
[2]*Department of Chemistry and Bioscience, Aalborg University, Aalborg 9220, Denmark*
[3]*Physics of AmoRphous and Inorganic Solids Laboratory (PARISlab), Department of Civil and Environmental Engineering,
University of California, Los Angeles, California 90095, USA*

The dynamics of atoms plays a key role in governing various dynamical and transport properties of glasses. However, it remains elusive which structural features (if any) control atom dynamics in glasses. Here, based on million-atom molecular dynamics simulations and classification-based machine learning, we extract a needle in a haystack by identifying a local, nonintuitive structural signature (a revised version of the recently developed softness metric) that governs glass dynamics. We do so by investigating the ion mobility in sodium silicate glasses—a realistic, archetypal glass—finding that the sodium ion mobility is largely encoded in its initial softness, wherein softer Na atoms exhibit higher mobility. Importantly, our approach allows us to interpret the machine-learned softness metric and thus elucidate the atomistic origin of the ion mobility. Namely, we find that Na mobility is anticorrelated with the local density of defect oxygen neighbors that are located between the nearest two coordination shells. This local packing order offers a potential path to develop glass formulations with tailored dynamical properties. Finally, we demonstrate that the softness is strongly anticorrelated with the activation energy for Na atom reorganization.

I. INTRODUCTION

The origin and nature of glass dynamics—i.e., the dynamic motion of the atoms in the glassy state—have remained mysterious for centuries [1–3]. A prominent example of this mystery is manifested as the ubiquitous-yet-indefinite relaxation behaviors of glasses at room temperature [4–6]. Indeed, the dynamics of the atoms governs various dynamical and transport properties of the glass [7,8], including viscosity [9,10], thermal conductivity [11,12], and ion diffusivity [13,14]. In that regard, understanding the key structural features that control atom dynamics would facilitate the rational design of tailored glasses [15,16]. However, due to the complex and disordered nature of glass structures [17,18], pinpointing which structural features (if any) govern dynamics is essentially a needle-in-a-haystack problem [19–21] since intuitive structural metrics [e.g., local packing or coordination number (CN)] are often only weakly correlated with dynamics [22–24]. As a result, a long-standing debate exists about whether glass dynamics is in some way encoded in the static glass structure [25].

As an emergent thrust to discover hidden patterns in complex, multidimensional data [26–28], machine learning (ML) has become a paradigm to unveil the nature of the linkages between glass dynamics and its static structure—without the need for any prerequisite intuition regarding which structural feature(s) could be influential [25,29–31]. Schoenholz

et al. [31], Cubuk *et al.* [32,33], and Sussman *et al.* [34] recently used classification-based ML to extract a nonintuitive structural fingerprint (named *softness*) which is strongly correlated with the probability of a particle to exhibit some rearrangement upon loading or spontaneous relaxation. Nevertheless, due to the intrinsic complexity of the ML model, our understanding of how glass dynamics is controlled by its static structure is still limited [25,31]. Specifically, although a few studies revealed that more liquidlike local neighborhoods tend to enhance atom mobility [24,31,33], it remains elusive what types of structural features are key to determine its liquidlike level and therefore control atom mobility in glasses [35–38]. Moreover, as the ML approach has thus far been applied to only some simple and small glass systems that may not capture the complex chemistry of more realistic ionocovalent oxide glasses [39–42], little is known about the level of correlation between glass dynamics and its static structure in more complex real-world glasses [30–32].

Here, inspired by the softness approach [31–33], we introduce a slightly revised definition for softness (relying on logistic regression and radial features, see below)—which we recently proposed to successfully predict creep dynamics of silicate gels from their static structure [43]—and apply it to investigate ion mobility in sodium silicate glasses, an archetypal glass with relevance in various fields such as household windows [1,2], display screens [16,44], magmatic rocks [10], and battery electrolytes [45,46]. It is worth mentioning that, by conducting million-atom molecular dynamics (MD) simulations, we extend the softness approach to investigate a more realistic and larger glass system ($<10^4$ atoms) [32,35,39].

*happylife@ucla.edu

TABLE I. Interatomic potential parameters [47]. The superscript of each element is the element charge.

Interaction	A_{ij} (eV)	ρ_{ij} (Å)	C_{ij} (eV|Å^6)
$O^{-1.2}$–$O^{-1.2}$	1844.7458	0.343645	192.580
$Si^{+2.4}$–$O^{-1.2}$	13702.9050	0.193817	54.681
$Na^{+0.6}$–$O^{-1.2}$	4383.7555	0.243838	30.700

Indeed, we find that the Na atom mobility is largely encoded in its initial softness, where a softer Na atom exhibits higher mobility, and the predictive power of Na atom softness remains valid when extrapolating to higher-temperature or longer-time glass dynamics. Importantly, we demonstrate that the softness effectively captures the activation energy for Na atom reorganization, suggesting that the initial static structure can dictate the topography of the local energy landscape. Finally, the use of logistic regression allows us to interpret the ML softness metric. By decoding the softness, we conclude that the sodium ion mobility is highly controlled by the local density of defect oxygen neighbors that are located between the first and second coordination shells.

II. METHODS

A. Interatomic potential interaction in sodium silicate glasses

To establish our conclusions, we simulate the spontaneous relaxation process of a $(Na_2O)_{30}(SiO_2)_{70}$ glass. The interatomic potential adopted herein is the well-established Teter potential [14,47,48], which has been proven to offer an accurate description of various structural, dynamical, and thermodynamical properties of silicate glasses [10,12,48,49]. In general, ionocovalent glasses (e.g., sodium silicate glasses) can be well described by using only radial two-body interactions [12,50], and each pairwise interaction consists of both the long-range Coulombic interaction and the short-range interaction. The Coulombic interaction is evaluated by a damped shifted force model [51] with a damping parameter of 0.25 and a cutoff of 8 Å [52,53], and partial charge is used for each element [54] (see Table I). The short-range interactions of Si–Si, Si–Na, and Na–Na are set to zero, and a Buckingham-format potential is adopted to describe the short-range interaction of the other atom pairs (Si–O, O–O, and Na–O) [12,48,53]:

$$U_{ij} = A_{ij}\exp\left(-\frac{r_{ij}}{\rho_{ij}}\right) - \frac{C_{ij}}{r_{ij}^6}, \qquad (1)$$

where r_{ij} is the distance between each pair of atoms, and A_{ij}, ρ_{ij}, and C_{ij} are some parameters describing the short-range interactions (see Table I). A cutoff of 8 Å is consistently used for the short-range interactions [12,48]. Note that a repulsive term is introduced for small r_{ij} values to prevent atom overlap, known as the *Buckingham catastrophe* [52], and is calculated so that the modified potential and its derivative are both continuous [48,49].

B. Preparation of melt-quenched $(Na_2O)_{30}(SiO_2)_{70}$ glasses

We then prepare the $(Na_2O)_{30}(SiO_2)_{70}$ glasses by a melt-quenching MD simulation. First, we construct a large configuration that contains 1 million atoms (i.e., 205 800 Na atoms) in a cubic box with periodic boundary conditions and a side length of 241 Å, in agreement with the experimental density (2.466 g/cm^3) [48]. Note that, as an independent test configuration (see Sec. III C), we also construct a small 3000-atom system subjected to the same simulation protocol. The NVT ensemble is applied in the entire simulation process using a Nosé-Hoover thermostat [55], and the timestep is fixed as 1 fs. Note that the Nosé-Hoover thermostat generally offers realistic atom trajectories suitable for the statistical analyses in this paper [56]. The system is initially melted at 4000 K for 100 ps. The glass is prepared by melt quenching from 4000 to 400 K with a cooling rate of 1 K/ps, and the glass transition temperature T_f is ~2100 K (see Sec. S1.1 in the Supplemental Material [57]). Partial pair distribution functions of the simulated glass are computed as an initial static structural reference (see Sec. S1.2 in the Supplemental Material [57]). During the melt-quenching process, we take out the configurations at several selected temperatures, including 400, 600, 700, 800, 1000, 1500, 2000, and 2500 K, to performance spontaneous relaxation simulations under the selected temperatures.

C. Tracing Na atom motions in glasses at constant temperatures

Finally, using the prepared glass configurations, we conduct relaxation simulations at the selected temperatures and track the location of atoms (Na) over time. Specifically, we conduct short-time relaxation simulations at 400, 600, 800, 1000, 1500, 2000, and 2500 K, respectively, for 50 ps, and a long-time simulation at 700 K for 5 ns. Note that, if not specified, all the analyses conducted in the following are based on the relaxation simulation of the glass at 700 K during the initial 50 ps. This temperature is large enough to activate the motion of an Na atom but simultaneously low enough to ensure that Si and O network-forming atoms remain largely immobile within the time of the simulation (see Secs. S1.3 and S1.4 in the Supplemental Material [57]). All simulations are performed by using the LAMMPS code [58].

III. RESULTS

A. Mobile vs immobile Na atoms

Based on the trajectories of Na atoms, we identify herein those mobile Na atoms that can easily reorganize to new sites, from the immobile atoms that only vibrate around their original locations. Figure 1 shows the distribution of the displacement D of Na atoms at the end of the relaxation simulation. Here, D is calculated as the distance between the initial and final positions of the atom during the relaxation. Notably, the distribution profile features two peaks associated with two atom ensembles—namely, immobile ($D < D_0$) and mobile ($D \geqslant D_0$) Na atoms, respectively, wherein D_0 is the threshold displacement that distinguishably separates the two peaks (herein, $D_0 = 2$ Å, i.e., the local minimum between the two peaks), and the two ensembles represent the populations of Na atoms that are (i) simply vibrating while remaining trapped in their local pocket and (ii) Na atoms that have jumped to another pocket during the time of the simulation, respectively [13]. In the following, we use this threshold D_0 to classify Na atoms as immobile (low displacement) or mobile (high
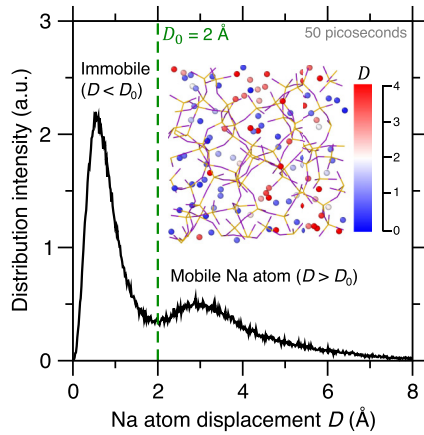
FIG. 1. Distribution of the displacement D of Na atoms in a $(Na_2O)_{30}(SiO_2)_{70}$ glass at the end of the relaxation simulation. The system contains 205 800 Na atoms and is relaxed at a constant temperature (700 K) and volume for 50 ps. The green dash refers to a selected threshold displacement $D_0 = 2$ Å that discriminates mobile Na atoms from immobile Na atoms. The inset is a colormap of the displacement of Na atoms in the bonded silicate network.

displacement). Based on this threshold, ~39.7% Na atoms are classified as mobile during the relaxation. Note, however, that the following analysis is largely insensitive to small variations of the selected threshold and does not significantly depend on the arbitrary choice of this threshold displacement (see Sec. S2 in the Supplemental Material [57]). Finally, it should be pointed out that, compared with other metrics of atom mobility (e.g., nonaffine squared displacement [43,59]), the present D metric is simpler but cannot identify mobile Na atoms exhibiting complex diffusion paths back to their initial

positions—which turn out to be rarely likely in the present system (see Sec. S3.1 in the Supplemental Material [57]).

B. ML Na atom softness by mobility classification

We now investigate whether the propensity for an Na atom to be mobile or immobile (i.e., a dynamic property) could be in some way encoded in its initial static structure. To this end, following the example of the softness approach [31–33], we construct by ML a structural quantity that is correlated with the mobility of Na atoms during the relaxation process. Each step of the ML process is detailed in Sec. S2.1 in the Supplemental Material [57] (see also Refs. [60,61] therein). Briefly, based on the present simulation, we first build a dataset that contains 205 800 Na atoms from the large $(Na_2O)_{30}(SiO_2)_{70}$ glass configuration simulated herein, where 70% of the Na atoms serve as a training set. Note that the size of the training set has been proven to be large enough to eliminate the risk of sample deficiency for the ML model training (see Sec. S2.2 in the Supplemental Material [57]). Then all Na atoms are labeled as mobile ($D \geqslant D_0$) or immobile ($D < D_0$) by comparing their displacement D with the threshold displacement D_0 at the end of the relaxation simulation. We then train a classifier to identify an optimal classification hyperplane that separates mobile from immobile Na atoms in a standardized N_r-dimensional classification space, as illustrated in Fig. 2(a). Here, the N_r input features (i.e., the classification space) of the classifier are constructed by computing (based on the initial static structure before the relaxation simulation) a series of N_r radial order parameters $G(i; r)$ that describe the local oxygen density of each Na atom i at different distances r [33,43]:

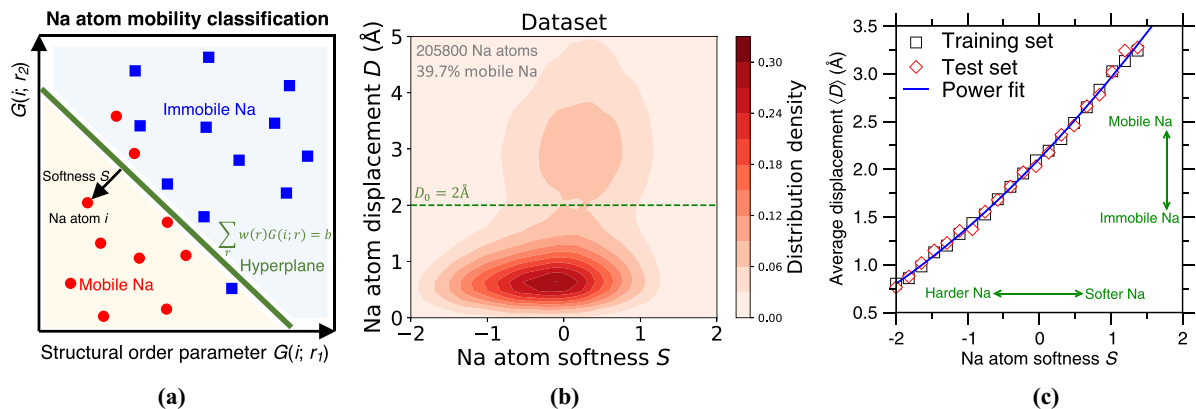$$G(i; r) = \sum_j \exp\left[-\frac{(R_{ij} - r)^2}{L^2}\right], \qquad (2)$$

FIG. 2. (a) Schematic of the classification model used to separate mobile Na atoms (red circle) from immobile Na atoms (blue square) using a classification hyperplane (green line). The input features are constructed by a series of N_r structural order parameters $G(i; r)$ that describe the local oxygen density of each Na atom i at different distances r [see Eq. (2)]. For illustration purposes, here, two input features associated with the distances $r_1 = 2.36$ Å and $r_2 = 4.68$ Å (i.e., the average distance of the first and second coordination shell, respectively) are selected to represent the N_r-dimensional feature space. The hyperplane is identified by logistic regression. (b) Distribution density of the final displacement D and initial softness S Na atoms. The softness S is defined as the orthogonal distance between the atom and the hyperplane in classification space [see (a)]. Mobile and immobile atoms correspond to positive and negative S, respectively. The dataset contains 205 800 Na atoms from a large $(Na_2O)_{30}(SiO_2)_{70}$ configuration with 39.7% mobile Na ($D \geqslant D_0$) and is randomly divided into the training (70%) and test sets (30%). (c) Final average Na atom displacement $\langle D \rangle$ of the training and test sets as a function of their initial softness S. The blue line is a power fit to guide the eye.

where j refers to the neighbor O atom of Na atom i within a cutoff distance R_G (here, $R_G = 8$ Å [33,62]), R_{ij} is the distance between the atom i and j, and L is the standard deviation of the Gaussian functions centered around r (here, $L = 0.2$ Å [33,62]). Overall, we calculate for each Na atom a series of $G(i; r)$ ranging from $r = 1.6$ to 6.4 Å with an increment of 0.3 Å [33,62], and the ensemble of these metrics offers an unbiased fingerprint of the local radial order around each Na atom.

For each Na atom, we extract a synthetic, local structural quantity softness from the classifier, where the softness S is defined as the orthogonal distance between the atom and the hyperplane in classification space [see Fig. 2(a)], and mobile and immobile atoms correspond to positive and negative values of S, respectively. Unlike the original softness approach that uses as inputs both radial and angular order features [31–33], we here solely focus on radial features capturing two-body correlations around each Na atom. This is key to ensure that our softness metric remains highly interpretable (see Sec. III D). Note that, since the Na–O interaction is nondirectional, incorporating angular three-body order parameters does not notably increase the classification accuracy (see Sec. S3.2 in the Supplemental Material [57]), in agreement with previous studies in Lennard-Jones systems [31,34]. In that regard, limiting the number of input features also ensures that the model does not become overfitted. Moreover, as an alternative to the support vector machine-based classifying technique adopted by the original softness approach [31–33], we use logistic regression to build the classifier [63], which offers great model simplicity, accuracy, and interpretability [43,63] (see Sec. S2.1 in the Supplemental Material [57]). Indeed, logistic regression directly provides the probability of a given atom to be mobile or immobile. In addition, it embeds regularization to limit the risk of overfitting. Importantly, the classification hyperplane determined by logistic regression is linear, which makes it possible to easily assess the importance of each feature. We also expect that the linear nature of the hyperplane is key to enhance the extrapolability of the classification model.

C. Softness governing Na atom dynamics

We now analyze the outcome of the classification. Figure 2(b) shows the distribution density of the final displacement D and initial softness S of Na atoms. We find that the softness sign ($S > 0$ or $S < 0$) can properly separate mobile ($D \geqslant D_0$) and immobile ($D < D_0$) Na atoms with a decent classification accuracy of ~63% for both the training and test sets. Note that the accuracy remains limited as many soft Na atoms ($S > 0$) remain trapped in the cage effect ($D < D_0$) under the fairly low relaxation temperature selected herein (see Sec. IV B) [13]. In contrast, at elevated temperature, the static structure tends to lose its predictivity of the long-time glass dynamics as the system quickly loses the memory of its initial structure [25]. Further, Fig. 2(c) shows the final average Na atom displacement $\langle D \rangle$ of both the training and test sets as a function of their initial softness S. Interestingly, we find that the magnitude of Na atom displacement features a power law dependance on softness, where softer Na atoms exhibit larger displacement during the relaxation, and vice versa, as

described in the form of $D \propto S^\lambda$ by shifting S to the positive axis and assigning a fitting exponent to S. This power law correlation is likely rooted in an intimate link between Na atom softness and the energy barrier for the atom to rearrange during relaxation (see Sec. IV C), which echoes recent studies that reveal a generic power law relationship between particle displacement D and the associated energy barrier E_b to overcome in disordered materials, namely, $D \propto E_b^\lambda$ [64,65].

For Na atoms belonging to the test set, it is notable that the degree of correlation remains high between their softness and dynamics. Figure 3(a) shows a snapshot of the predicted Na atom softness in an additional 3000-atom $(Na_2O)_{30}(Si O_2)_{70}$ glass that is simulated herein as a fully independent test set. Note that the test glass is prepared by the same simulation protocol as that of the large training configuration (see Sec. II), and all the analyses herein are based on its relaxation simulation after 50 ps at 700 K. The distribution of softness (both for all Na atoms and for mobile Na atoms in the glass) is provided in Fig. 3(b). We find that the classification accuracy is satisfactory as ~64% of the mobile Na atoms indeed exhibit a positive softness ($S > 0$). Further, we calculate the probability $P_R(S)$ of an Na atom to rearrange ($D \geqslant D_0$) as a function of its initial softness S [Fig. 3(c)]. Interestingly, we find that $P_R(S)$ exhibits an exponential dependance on S, as it is following an activated process [66,67]:

$$P_R(S) = P_0 \exp(\beta S), \tag{3}$$

where P_0 and β are fitting parameters. In accordance with the power law correlation between the final displacement D and initial softness S of Na atoms [see Fig. 2(c)], this exponential correlation between $P_R(S)$ and S suggests that the structural quantity S is closely related to (and might be indicative of) the energy barrier associated with Na atom rearrangement (see Sec. IV C) [31,42,68], as suggested in a recent study of the creep dynamics of gels [43]. Note that softness is calculated based on the sole knowledge of the initial structure, whereas the Na atom displacement is computed at the end of the relaxation simulation. The high degree of correlation between initial softness and final displacement clearly illustrates the intimate link between glass dynamics and its initial static structure.

D. Structural interpretation of Na atom softness

Finally, we discuss the structural interpretation of the ML softness metric. Indeed, the hyperplane created by logistic regression can be expressed as a linear equation of each of the features as [see Fig. 2(a)]

$$\Sigma_r w(r) G(i; r) = b, \tag{4}$$

wherein $w(r)$ and b are the coefficients and the bias of the logistic regression model, respectively. Note that, all input features $G(i; r)$ have been standardized (before training) so that the coefficients are directly indicative of the relative importance of each feature in the classification. Namely, a large absolute value for $w(r)$ refers to a fairly orthogonal hyperplane to the axis associated with the corresponding feature $G(i; r)$. In addition, the positive and negative signs of the coefficients $w(r)$ are informative as they indicate that increasing
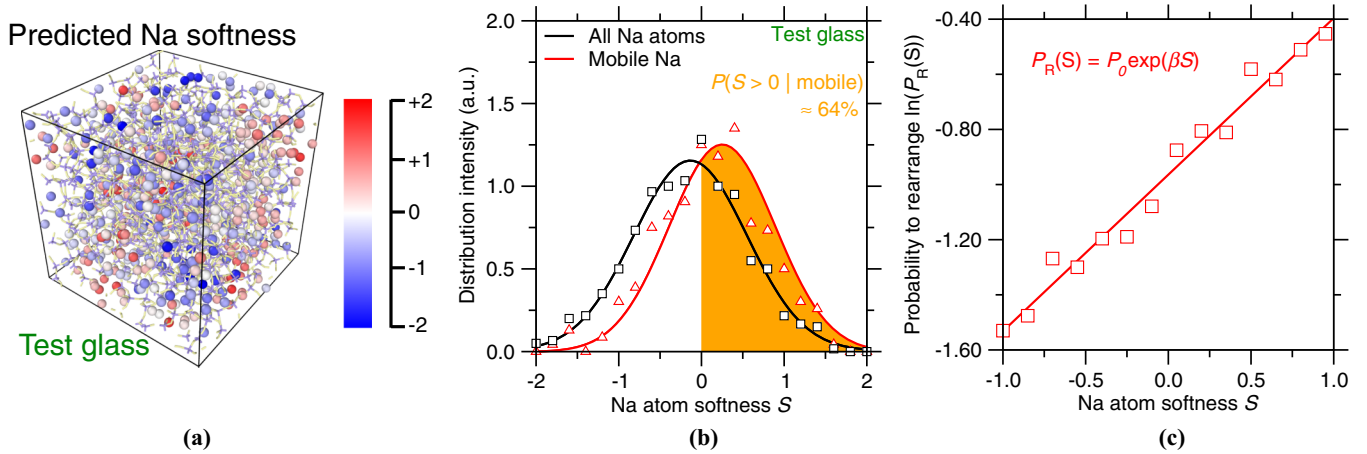
(a)   **(b)**   **(c)**

FIG. 3. (a) Snapshot of the predicted Na atom softness S for a new, independent test $(Na_2O)_{30}(SiO_2)_{70}$ glass. The system contains 600 Na atoms as a test set. (b) Distribution of the softness of all Na atoms (black) and mobile Na atoms (red) in the glass. The orange area represents the properly predicted soft Na atoms ($S > 0$) within the mobile Na atoms. (c) Logarithm of the probability $\ln[P_R(S)]$ of an Na atom to rearrange ($D \geqslant D_0$) as a function of its initial softness S. The red line is an exponential fit following Eq. (3).

values of the feature $G(i; r)$ tend to result in increased and decreased softness values, respectively.

Figure 4(a) shows the coefficients $w(r)$ of the logistic regression classifier as a function of the distance r, wherein the absolute value of $w(r)$ denotes how influential the feature $G(i; r)$ is on determining the atom softness. We find that the most influential feature is associated with the distance r_m that corresponds to the region that is located between the peak positions r_1 and r_2 of, respectively, the first and second coordination shells of the Na–O partial pair distribution function $g_{Na-O}(r)$ (see the upper panel of Fig. 4). Note that $w(r)$ is negative at the distance r_m as well as at all other distances. Although the absolute values of $w(r)$ at other distances are smaller and approach zero when r is larger than r_2, we notice

that the features $G(i; r)$ that are associated with distances r that are close to r_m (between r_1 and r_2) contribute significantly more than other features to determine softness (see the gray window in Fig. 4). Namely, a defect oxygen neighbor located in this extent of distances (i.e., between the first and second coordination shells) tends to greatly reduce the mobility of the Na atom [see blue particle in Fig. 4(a)], although all oxygen neighbors within the first two coordination shells synergically reduce the mobility of the central Na atom. The key role played by the defect oxygen neighbors at the intershell region is to occupy those potential empty jumping sites around the central Na atom to block the motion of the Na atom within the displacement threshold ($D < D_0$) (see Supplemental Material [57]).
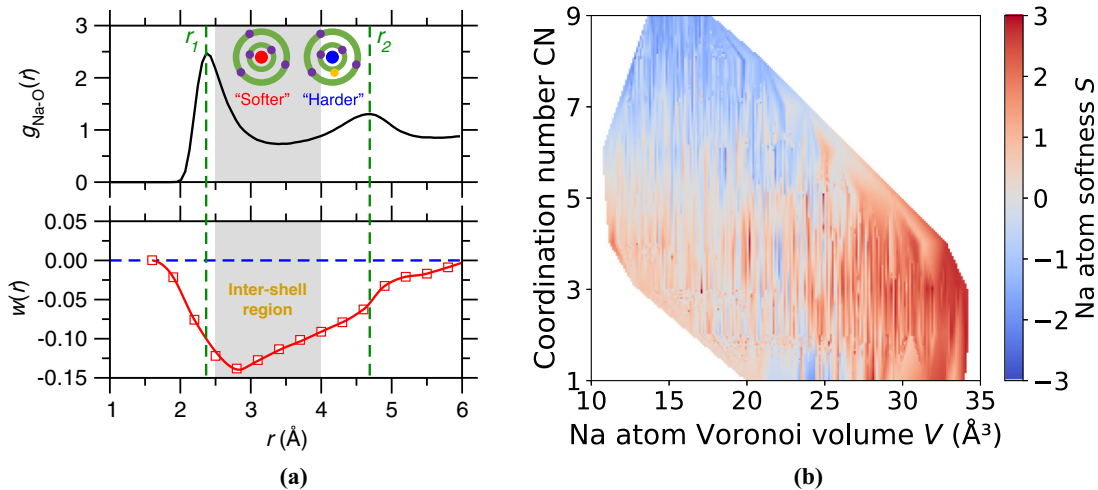

(a)   **(b)**

FIG. 4. (a) Weight coefficient $w(r)$ of the classification hyperplane [see Fig. 2(a)] at different distances r. The red line is to guide the eyes. The partial Na–O pair distribution function $g_{Na-O}(r)$ of the glass is added in the top panel as reference. The distance r_1 and r_2 are associated with the peak position of the first and second coordination shells of $g_{Na-O}(r)$, respectively. The gray window indicates the range of large weights. The inset illustrates the local oxygen (purple sphere) environments around (i) a soft Na atom (red sphere) and (ii) a harder Na atom (blue sphere) with an extra O atom (gold sphere) between the first and second coordination shells (green halo). (b) Na atom softness S as a function of their Voronoi volume V and coordination number (CN). The color coding is based on a linear interpolation between the datapoints in the Na atom dataset.
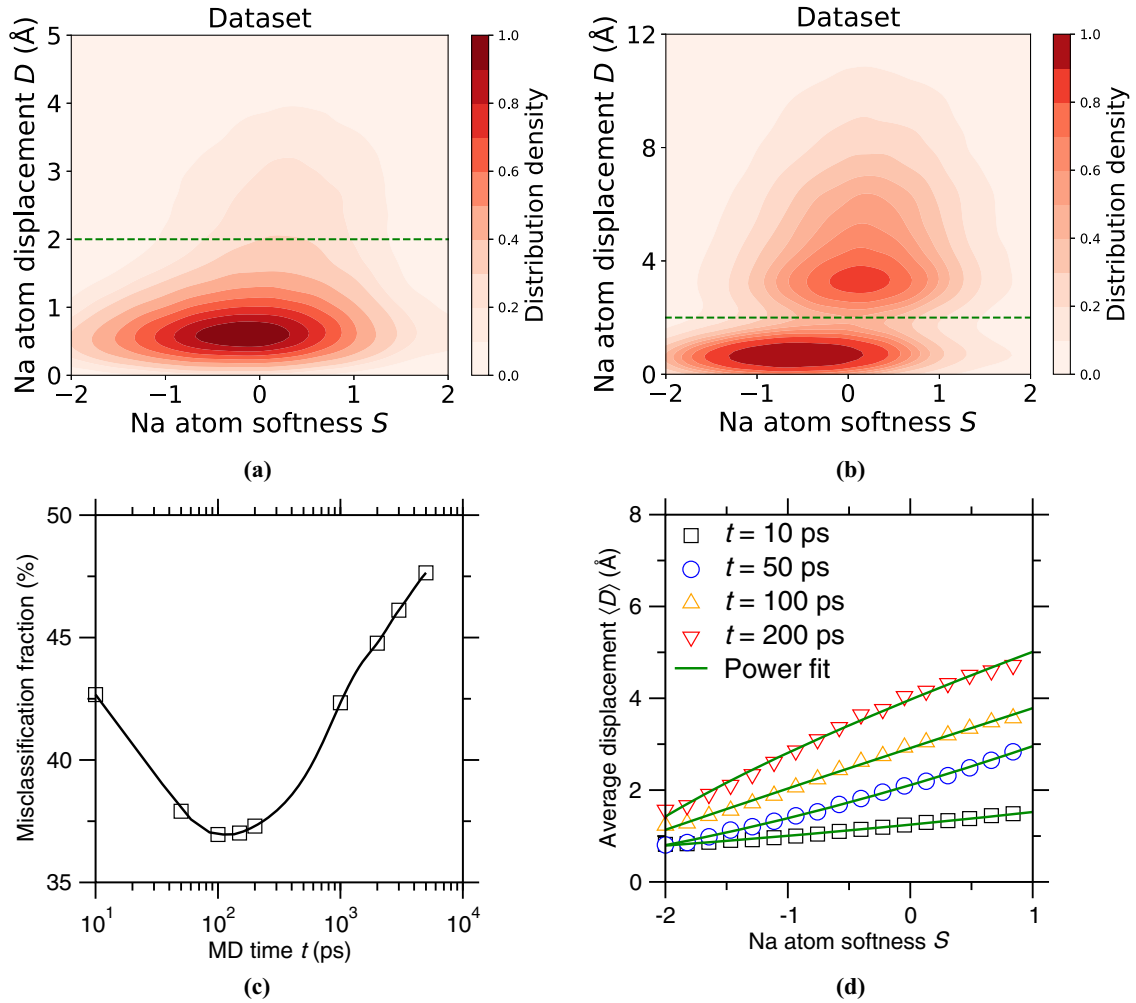
FIG. 5. Distribution density of the initial softness S and final displacement D of Na atoms at (a) 10 ps and (b) 200 ps, respectively, wherein S is computed from the displacement at 50 ps. The green dash refers to the selected displacement threshold $D_0 = 2$ Å for Na atom reorganization. (c) Misclassification fraction as a function of relaxation time ranging from 10 to 5000 ps. The line is a guide to the eye. (d) Average displacement as a function of Na atom softness at 10, 50, 100, and 200 ps, respectively. The lines are power fit to guide the eyes.

These results are consistent with free volume theory [13,14,47]. Indeed, closed-packed structures with many oxygen neighbors are associated with low local free volume, wherein the central Na atom exhibits very limited mobility. In contrast, more loosely packed structures exhibiting less oxygen neighbors tend to show more potential empty jumping sites around them, which promotes Na atom mobility [see red particle in Fig. 4(a)]. Further, Fig. 4(b) illustrates the dependance of the softness S of Na atoms on their Voronoi volume V and CN. Overall, larger CN and smaller V values tend to favor smaller softness. However, we nevertheless observe that softness is a complex, nonmonotonic function of CN and V. Indeed, we find that the classifier trained by the sole knowledge of the Na atom Voronoi volume offers a very limited accuracy of ∼50% as compared with that offered by the softness metric (∼63% accuracy, see Supplemental Material for details [57]). Similarly, training a classifier based on the sole knowledge of the Na atom CN yields an accuracy of ∼52%, wherein both low- and high-coordination atoms are very likely to be classified as soft (see Supplemental Material for details [57]). This indicates that, although they offer an in-

tuitive interpretation of the origin of Na mobility, the CN and Voronoi volume metrics do not fully capture the propensity of Na to reorganize. This exemplifies the benefit of using an unbiased ML approach to build the set of input features since intuitive structural features show only limited correlation with dynamical properties.

IV. DISCUSSION

A. Predictive power of Na atom softness in its time-dependent displacement

We now evaluate whether the Na atom softness computed at a fixed time duration can predict the time-dependent displacement. Figures 5(a) and 5(b) show the distribution density of the initial softness S and final displacement D of Na atoms at 10 and 200 ps, respectively, wherein S is computed from the displacement at 50 ps. We find that, after a duration of 200 ps, the initial softness remains predictive to discriminate mobile Na atoms (i.e., $D > 2$ Å) from immobile Na atoms (i.e., $D < 2$ Å), with a classification accuracy of 64% slightly higher than that offered at 50 ps. Figure 5(c) further provides
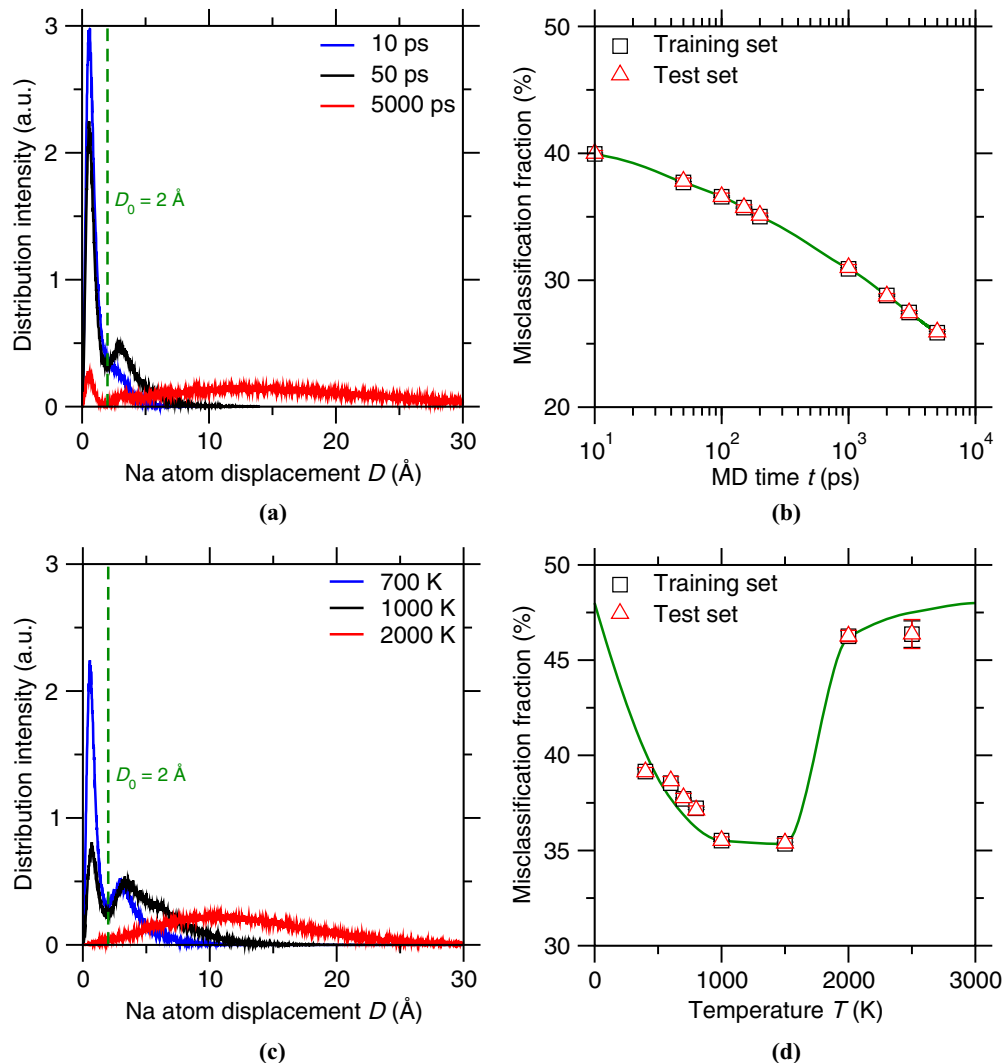
FIG. 6. (a) The distribution of Na atom displacement at 700 K after a duration of 10, 50, and 5000 ps, respectively. The green dash refers to the selected displacement threshold $D_0 = 2$ Å for Na atom reorganization. (b) Misclassification fraction as a function of relaxation time for both the training and test set, where 10 random training-test splits are performed at each selected time for statistical average. The green line is a guide to the eye. (c) The distribution of Na atom displacement after a duration of 50 ps at 700, 1000, and 2000 K, respectively. (d) Misclassification fraction as a function of the relaxation temperature for both the training and test set, where 10 random training-test splits are performed at each selected time for statistical average. The green line is a guide to the eye.

the misclassification fraction as a function of relaxation time ranging from 10 to 5000 ps. It is notable that the classification accuracy shows a quadratic dependance on the relaxation time t and exhibits a maximum at $t = \sim 200$ ps. Indeed, at short-term relaxation regime ($t < 200$ ps), soft Na atoms gradually reorganize to be mobile and consequently promote the classification accuracy; while at long-term relaxation regime ($t > 200$ ps), the local structure gradually loses its initial memory so that the initial softness eventually fails to predict atom mobility. We nevertheless find that, after a long relaxation time up to 1 ns, the softness metric remains satisfactory to predict Na atom mobility, with a classification accuracy of $\sim 60\%$, close to that offered at 50 ps, as a manifestation of the slow dynamics of Si and O atoms under the glassy state (see Sec. S1.3 in the Supplemental Material [57]). Finally, Fig. 5(d) shows the power law dependance of the average displacement of Na atoms on their softness after 10, 50, 100,

and 200 ps, respectively, where the power law varies and is largely dependent on the relaxation time (see Sec. III C), and apparently, longer relaxation time results in larger average displacement. Overall, these results demonstrate that the atom softness computed from short-term dynamics remains predictive when extrapolating to longer-term dynamics.

B. Temperature (and time) dependence of Na atom mobility on its static structure

Rather than the extrapolability of the computed softness metric (see Sec. IV A), We examine herein whether the softness approach itself (i.e., the classification-based ML) remains valid for high-temperature (or long-time) dynamics, where the Na atoms undergo pronounced displacement. Figure 6(a) shows the distribution of Na atom displacement at 10, 50, and 5000 ps, respectively. As expected, more and more Na
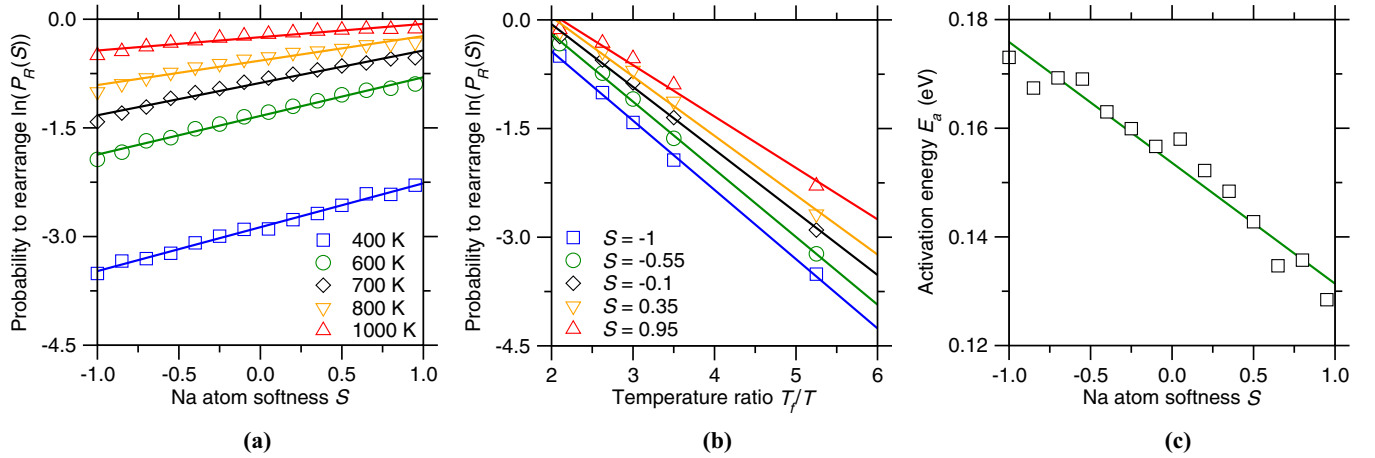
FIG. 7. (a) The logarithm of probability to rearrange $\ln[P_R(S)]$ as a function of Na atom softness S at 400, 600, 700, 800, and 1000 K, respectively. The lines are exponential fittings following Eq. (3). (b) $\ln[P_R(S)]$ as a function of temperature ratio T_f/T for Na atoms exhibiting the same softness $S = -1, -0.55, -0.1, 0.35$, and 0.95, respectively, where $T_f = 2100$ K is the fictive temperature. The lines are exponential fittings following Eq. (5). (c) Activation energy E_a estimated from Eq. (5) as a function of S. The green line is a linear fit following Eq. (6).

atoms become mobile (i.e., $D > 2$ Å) as the relaxation time increases, and the mobile Na atoms account for 93.6% of the system after 5 ns when the system starts to enter into the diffusive regime (see Sec. S1.3 in the Supplemental Material [57]). By applying the softness approach at different durations (see Sec. S2.3 in the Supplemental Material [57]), Fig. 6(b) provides the misclassification fraction as a function of relaxation time for both the training and test set, where 10 random training-test splits are performed at each selected time for statistical average. We find that the misclassification fraction gradually decreases from 40 to 25% during a relaxation time of 5 ns because of more and more reorganized soft Na atoms—in contrast to the slow dynamics of silicate network under the glassy state (see Sec. S1.3 in the Supplemental Material [57]). These results demonstrate the validity of the softness approach when applied to long-time glassy dynamics—if the local structure does not lose its initial memory, in harmony with the recent study that predicts the long-term creep dynamics of gels from its static structure [43].

We now investigate the validity of the softness approach at elevated temperatures. Figure 6(c) shows the distribution of Na atom displacement during 50 ps at 700, 1000, and 2000 K, respectively. We find that 98.9% of Na atoms reorganize and jump out of their cages when the system temperature increases to 2000 K, i.e., at the vicinity of glass transition temperature $T_f = 2100$ K (see Sec. S1.1 in the Supplemental Material [57]). By applying the softness approach at different temperature (see Sec. S2.4 in the Supplemental Material [57]), Fig. 6(d) shows the misclassification fraction as a function of the relaxation temperature for both the training and test set, where 10 random training-test splits are performed at each selected temperature for statistical average. Interestingly, we find that the softness approach exhibits a minimum misclassification fraction at ~1500 K. Indeed, at higher temperature, the classification accuracy rapidly deteriorates due to the pronounced rearrangement of local structures (see Sec. S1.4 in the Supplemental Material [57]); while at lower temperature, less soft Na atoms are activated to reorganize to suppress the

classification accuracy—although the local structure remains largely unchanged in the short-time relaxation. Overall, these results suggest that the softness approach would eventually lose its predictivity in high-temperature (or long-time) dynamics, as the system gradually evolves away from its initial static structure.

Note that, unlike the general validity of the softness approach for glass dynamics within the simulation time [see Fig. 6(b)], the softness computed at a specific temperature and time generally exhibit a limited extrapolability at the vicinity of the relaxation temperature and time [see Fig. 5(c)], as the classifier is trained specifically to maximize the classification accuracy at the training relaxation condition, regardless of the fact that the resultant classification hyperplane remains the same weight shape as that shown in Fig. 4(a) (see Secs. S2.3 and S2.4 in the Supplemental Material [57]).

C. Correlation between Na atom softness and its activation energy

Relying on the temperature-dependent glass dynamics, we discuss herein the nature of the linkage between Na atom softness and its activation energy. To this end, we adopt the Na atom softness computed at 700 K to predict glassy dynamics at various temperatures, where the temperatures are selected at the vicinity of 700 K to ensure the softness extrapolability (see Sec. S2.4 in the Supplemental Material [57]). Figure 7(a) provides the logarithm of probability to rearrange $\ln[P_R(S)]$ as a function of Na atom softness S at 400, 600, 700, 800, and 1000 K, respectively. Like Fig. 3(c), at all the different temperatures, the probability of Na atom rearrangement exhibits an exponential dependance on its initial softness, and higher temperature results in orders of magnitude larger probability to rearrange. Figure 7(b) further shows the probability to rearrange $\ln[P_R(S)]$ as a function of temperature T for Na atoms exhibiting the same softness level ranging from -1 to 1. It is interesting that, at all the different softness levels, the probability of Na atom rearrangement exhibits an exponential
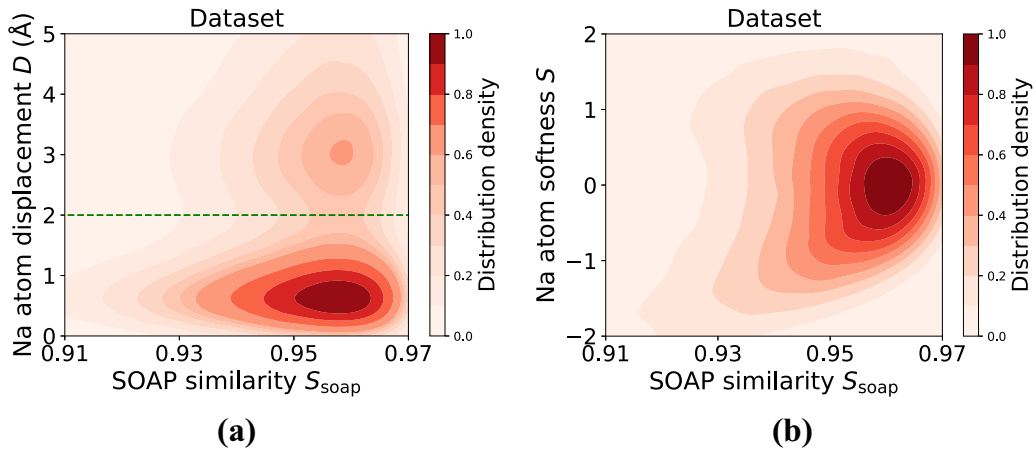
FIG. 8. (a) Distribution density of the final displacement D and initial SOAP similarity S_{soap} of Na atoms. The green dash refers to the selected displacement threshold $D_0 = 2$ Å for Na atom reorganization. (b) Distribution density of the initial softness S and initial SOAP similarity S_{soap} of Na atoms.

dependance on the system temperature T, as described by the Arrhenius-form activation process [31]:

$$P_R(S) = P_0 \exp\left[\frac{E_a(S)}{kT}\right], \tag{5}$$

where P_0 is a pre-exponential fitting parameter, k is the Boltzmann constant, and E_a is the activation energy. Figure 7(c) shows the activation energy E_a estimated from Eq. (5) as a function of Na atom softness S. Notably, E_a exhibits a linear scaling with respect to S, namely,

$$E_a = eS + e_0, \tag{6}$$

where e and e_0 are fitting parameters, and $e < 0$. Indeed, softer Na atoms (i.e., Na atoms exhibiting larger S) are prone to rearrange, suggesting lower energy barriers accessible to the atom rearrangement. This strong linear correlation between Na atom softness and its activation energy suggests that the local energy landscape of a glass system is largely encoded in its initial static structure.

D. Correlation between Na atom mobility and their SOAP atomic similarity

Finally, it is particularly of our interest to compare the softness approach with another method proposed to represent the atomic neighborhood environment, called Smooth Overlap of Atomic Positions (SOAP). Unlike the softness approach that directly extracts a local structural descriptor $S(i)$ for Na atom i, the SOAP approach defines the similarity $S_{soap}(i, j)$ of any two oxygen-neighborhood environments associated to Na atoms i and j, where the Na–O packing environment of Na atom i is described by a vector $q_{soap}(i)$ consisting of normalized SOAP many-body descriptors $\{p(i)\}$ (see Sec. S3.2 in the Supplemental Material [57])—in analogy to the radial two-body features $\{G(i)\}$ [see Eq. (2)] in the softness approach but much more complex. More technical details can be found in Ref. [69]. The atomic similarity $S_{soap}(i, j)$ between Na atoms i and j is computed herein as the dot product of $q_{soap}(i)$ and $q_{soap}(j)$ [69,70]:

$$S_{soap}(i, j) = q_{soap}(i) \cdot q_{soap}(j), \tag{7}$$

where $S_{soap}(i, j)$ ranges from 0 to 1 which represent, respectively, the low and high limits of the degree of atomic similarity between i and j. Note that, when using SOAP many-body descriptors $q_{soap}(i)$ as input features in the softness approach, we notice a slight enhancement of classification accuracy from ~63% to ~66% (see Sec. S3.2 in the Supplemental Material [57])—in accordance with the greatly enhanced model complexity—suggesting the dominant role of radial two-body features in describing the Na–O atomic neighborhood environment.

Based on the definition of $S_{soap}(i, j)$, we construct herein a structural metric SOAP similarity $S_{soap}(i)$ for each Na atom i, by averaging $S_{soap}(i, j)$ over all Na atoms j that exhibit the top 10% displacement (i.e., $D > 4.6$ Å herein) after a duration of 50 ps at 700 K, namely,

$$S_{soap}(i) = \langle S_{soap}(i, j) \rangle_j, \tag{8}$$

where $\langle \cdot \rangle_j$ denotes the average operator over j. Figure 8(a) shows the distribution density of the final displacement D and initial SOAP similarity S_{soap} of Na atoms. We find that, as S_{soap} decreases, Na atoms exhibit more confined displacement and gradually become immobile (i.e., $D < 2$ Å), in analogy to the correlation between the final displacement D and initial softness S of Na atoms [see Fig. 2(b)]. Further, Fig. 8(c) shows the distribution density of the initial softness S and initial SOAP similarity S_{soap} of Na atoms. Indeed, we find that the Na atoms that exhibit smaller S_{soap} are more likely to be harder atoms (i.e., atoms with smaller softness). This close correlation between S and S_{soap} echoes the fact that their definitions are similarly built upon a distance nature, that is, a similarity distance of the atomic neighborhood environment from a predefined environment reference [see Fig. 2(a)]. Overall, these results establish a close correlation between Na atom mobility and their SOAP atomic similarity, suggesting an intimate linkage between the distance nature of S and S_{soap}.

V. CONCLUSIONS

Overall, these results highlight the ability of ML to analyze large amounts of complex data and decode previously

hidden correlations—here, between the dynamics of a glass and its initial static structure. It is notable that our approach allows us to predict the dynamics of a realistic, complex oxide glass based on the sole knowledge of the ML softness metric. The interpretation of the softness metric defined herein [see Fig. 4(a)] suggests that the mobility of sodium atoms in silicate glasses is strongly anticorrelated with the local density of defect oxygen neighbors that are located between the first and second coordination shells. ML therefore offers a promising route to decode the complex relationship between structure and properties in disordered, out-of-equilibrium phases.

[1] *Springer Handbook of Glass*, edited by J. D. Musgraves, J. Hu, and L. Calvez (Springer, Cham, 2019).

[2] J. C. Mauro and E. D. Zanotto, Two centuries of glass research: Historical trends, current status, and grand challenges for the future, Int. J. Appl. Glass Sci. **5**, 313 (2014).

[3] J. C. Mauro, Decoding the glass genome, Curr. Opin. Solid State Mater. Sci. **22**, 58 (2018).

[4] R. C. Welch, J. R. Smith, M. Potuzak, X. Guo, B. F. Bowden, T. J. Kiczenski, D. C. Allan, E. A. King, A. J. Ellison, and J. C. Mauro, Dynamics of Glass Relaxation at Room Temperature, Phys. Rev. Lett. **110**, 265901 (2013).

[5] Y. Yu, M. Wang, D. Zhang, B. Wang, G. Sant, and M. Bauchy, Stretched Exponential Relaxation of Glasses at Low Temperature, Phys. Rev. Lett. **115**, 165901 (2015).

[6] Y. Yu, M. Wang, M. M. Smedskjaer, J. C. Mauro, G. Sant, and M. Bauchy, Thermometer Effect: Origin of the Mixed Alkali Effect in Glass Relaxation, Phys. Rev. Lett. **119**, 095501 (2017).

[7] *Molecular Dynamics Simulations of Disordered Materials: From Network Glasses to Phase-Change Memory Alloys*, edited by C. Massobrio, J. Du, M. Bernasconi, and P. S. Salmon (Springer, Cham, 2015).

[8] M. Bauchy, Deciphering the atomic genome of glasses by topological constraint theory and molecular dynamics: A review, Comput. Mater. Sci. **159**, 95 (2019).

[9] J. C. Mauro, Y. Yue, A. J. Ellison, P. K. Gupta, and D. C. Allan, Viscosity of glass-forming liquids, Proc. Natl. Acad. Sci. USA **106**, 19780 (2009).

[10] M. Bauchy, B. Guillot, M. Micoulaut, and N. Sator, Viscosity and viscosity anomalies of model silicates and magmas: A numerical investigation, Chem. Geol. **346**, 47 (2013).

[11] S. S. Sørensen, M. B. Østergaard, M. Stepniewska, H. Johra, Y. Yue, and M. M. Smedskjaer, Metal–organic framework glasses possess higher thermal conductivity than their crystalline counterparts, ACS Appl. Mater. Interfaces **12**, 18893 (2020).

[12] M. Bauchy, Structural, vibrational, and thermal properties of densified silicates: Insights from molecular dynamics, J. Chem. Phys. **137**, 044510 (2012).

[13] M. Bauchy and M. Micoulaut, From pockets to channels: Density-controlled diffusion in sodium silicates, Phys. Rev. B **83**, 184118 (2011).

[14] A. N. Cormack, J. Du, and T. R. Zeitler, Sodium ion migration mechanisms in silicate glasses probed by molecular dynamics simulations, J. NonCryst. Solids **323**, 147 (2003).

[15] J. C. Mauro, A. Tandia, K. D. Vargheese, Y. Z. Mauro, and M. M. Smedskjaer, Accelerating the design of functional glasses through modeling, Chem. Mater. **28**, 4267 (2016).

[16] M. C. Onbaşlı, A. Tandia, and J. C. Mauro, Mechanical and compositional design of high-strength Corning Gorilla® glass, in *Handbook of Materials Modeling: Applications: Current and Emerging Materials*, edited by W. Andreoni and S. Yip (Springer, Cham, 2020), pp. 1997–2019.

[17] E. D. Zanotto and F. A. B. Coutinho, How many non-crystalline solids can be made from all the elements of the periodic table? J. NonCryst. Solids **347**, 285 (2004).

[18] K. Binder and W. Kob, *Glassy Materials and Disordered Solids: An Introduction to Their Statistical Mechanics* (World Scientific, Singapore, 2011).

[19] S. S. Sørensen, C. A. N. Biscio, M. Bauchy, L. Fajstrup, and M. M. Smedskjaer, Revealing hidden medium-range order in amorphous materials using topological data analysis, Sci. Adv. **6**, eabc2320 (2020).

[20] M. A. Klatt, J. Lovrić, D. Chen, S. C. Kapfer, F. M. Schaller, P. W. A. Schönhöfer, B. S. Gardiner, A.-S. Smith, G. E. Schröder-Turk, and S. Torquato, Universal hidden order in amorphous cellular geometries, Nat. Commun. **10**, 811 (2019).

[21] M. Mungan, S. Sastry, K. Dahmen, and I. Regev, Networks and Hierarchies: How Amorphous Materials Learn to Remember, Phys. Rev. Lett. **123**, 178002 (2019).

[22] R. L. Jack, A. J. Dunleavy, and C. P. Royall, Information-Theoretic Measurements of Coupling between Structure and Dynamics in Glass Formers, Phys. Rev. Lett. **113**, 095703 (2014).

[23] A. Widmer-Cooper, P. Harrowell, and H. Fynewever, How Reproducible Are Dynamic Heterogeneities in a Supercooled Liquid? Phys. Rev. Lett. **93**, 135701 (2004).

[24] E. D. Cubuk, S. S. Schoenholz, E. Kaxiras, and A. J. Liu, Structural properties of defects in glassy liquids, J. Phys. Chem. B **120**, 6139 (2016).

[25] V. Bapst, T. Keck, A. Grabska-Barwińska, C. Donner, E. D. Cubuk, S. S. Schoenholz, A. Obika, A. W. R. Nelson, T. Back, D. Hassabis *et al.*, Unveiling the predictive power of static structure in glassy systems, Nat. Phys. **16**, 448 (2020).

[26] S. J. Russell and P. Norvig, *Artificial Intelligence: A Modern Approach*, 3rd ed. (Pearson Education, Inc., Upper Saddle River, 2016).

[27] H. Liu, Z. Fu, K. Yang, X. Xu, and M. Bauchy, Machine learning for glass science and engineering: a review, J. Non-Cryst. Solids: X **4**, 100036 (2019).

[28] R. Iten, T. Metger, H. Wilming, L. del Rio, and R. Renner, Discovering Physical Concepts with Neural Networks, Phys. Rev. Lett. **124**, 010508 (2020).

[29] G. Biroli, Machine learning glasses, Nat. Phys. **16**, 373 (2020).

[30] Z. Fan, J. Ding, and E. Ma, Machine learning bridges local static structure with multiple properties in metallic glasses, Mater. Today **40**, 48 (2020).

[31] S. S. Schoenholz, E. D. Cubuk, D. M. Sussman, E. Kaxiras, and A. J. Liu, A structural approach to relaxation in glassy liquids, Nat. Phys. **12**, 469 (2016).

[32] E. D. Cubuk, R. J. S. Ivancic, S. S. Schoenholz, D. J. Strickland, A. Basu, Z. S. Davidson, J. Fontaine, L. J. Hor, Y. R. Huang, Y. Jiang *et al.*, Structure-property relationships from universal signatures of plasticity in disordered solids, Science **358**, 1033 (2017).

[33] E. D. Cubuk, S. S. Schoenholz, J. M. Rieser, B. D. Malone, J. Rottler, D. J. Durian, E. Kaxiras, and A. J. Liu, Identifying Structural Flow Defects in Disordered Solids Using Machine-Learning Methods, Phys. Rev. Lett. **114**, 108001 (2015).

[34] D. M. Sussman, S. S. Schoenholz, E. D. Cubuk, and A. J. Liu, Disconnecting structure and dynamics in glassy thin films, Proc. Natl Acad. Sci. USA **114**, 10601 (2017).

[35] Q. Wang and A. Jain, A transferable machine-learning framework linking interstice distribution and plastic heterogeneity in metallic glasses, Nat. Commun. **10**, 5537 (2019).

[36] H. Tanaka, H. Tong, R. Shi, and J. Russo, Revealing key structural features hidden in liquids and glasses, Nat. Rev. Phys. **1**, 333 (2019).

[37] E. Boattini, S. Marín-Aguilar, S. Mitra, G. Foffi, F. Smallenburg, and L. Filion, Autonomously revealing hidden local structures in supercooled liquids, Nat. Commun. **11**, 5479 (2020).

[38] Q. Wang, J. Ding, L. Zhang, E. Podryabinkin, A. Shapeev, and E. Ma, Predicting the propensity for thermally activated β events in metallic glasses via interpretable machine learning, npj Comput. Mater. **6**, 194 (2020).

[39] E. D. Cubuk, A. J. Liu, E. Kaxiras, and S. S. Schoenholz, Unifying framework for strong and fragile liquids via machine learning: a study of liquid silica, arXiv:2008.09681.

[40] J. Du, Challenges in molecular dynamics simulations of multi-component oxide glasses, in *Molecular Dynamics Simulations of Disordered Materials: From Network Glasses to Phase-Change Memory Alloys*, edited by C. Massobrio, J. Du, M. Bernasconi, and P. S. Salmon (Springer, Cham, 2015), pp. 157–180.

[41] L. Huang and J. Kieffer, Challenges in Modeling Mixed Ionic-Covalent Glass Formers, in *Molecular Dynamics Simulations of Disordered Materials: From Network Glasses to Phase-Change Memory Alloys*, edited by C. Massobrio, J. Du, M. Bernasconi, and P. S. Salmon (Springer, Cham, 2015), pp. 87–112.

[42] X. Ma, Z. S. Davidson, T. Still, R. J. S. Ivancic, S. S. Schoenholz, A. J. Liu, and A. G. Yodh, Heterogeneous Activation, Local Structure, and Softness in Supercooled Colloidal Liquids, Phys. Rev. Lett. **122**, 028001 (2019).

[43] H. Liu, S. Xiao, L. Tang, E. Bao, E. Li, C. Yang, Z. Zhao, G. Sant, M. M. Smedskjaer, L. Guo *et al.*, Predicting the early-stage creep dynamics of gels from their static structure by machine learning, Acta Mater. **210**, 116817 (2021).

[44] M. C. Onbaşlı and J. C. Mauro, Modeling of glasses: an overview, in *Handbook of Materials Modeling*, edited by W. Andreoni and S. Yip (Springer, Cham, 2020), pp. 1977–1995.

[45] M. H. Braga, A. J. Murchison, J. A. Ferreira, P. Singh, and J. B. Goodenough, Glass-amorphous alkali-ion solid electrolytes and their performance in symmetrical cells, Energy Environ. Sci. **9**, 948 (2016).

[46] Z. A. Grady, C. J. Wilkinson, C. A. Randall, and J. C. Mauro, Emerging role of non-crystalline electrolytes in solid-state battery research, Front. Energy Res. **8**, 218 (2020).

[47] A. N. Cormack, J. Du, and T. R. Zeitler, Alkali ion migration mechanisms in silicate glasses probed by molecular dynamics simulations, Phys. Chem. Chem. Phys. **4**, 3193 (2002).

[48] J. Du and A. N. Cormack, The medium range structure of sodium silicate glasses: a molecular dynamics simulation, J. NonCryst. Solids **349**, 66 (2004).

[49] J. Du and L. R. Corrales, Compositional dependence of the first sharp diffraction peaks in alkali silicate glasses: A molecular dynamics study, J. NonCryst. Solids **352**, 3255 (2006).

[50] H. Liu, Z. Fu, Y. Li, N. F. A. Sabri, and M. Bauchy, Machine learning forcefield for silicate glasses, arXiv:1902.03486.

[51] C. J. Fennell and J. D. Gezelter, Is the Ewald summation still necessary? Pairwise alternatives to the accepted standard for long-range electrostatics, J. Chem. Phys. **124**, 234104 (2006).

[52] H. Liu, Z. Fu, K. Yang, X. Xu, and M. Bauchy, Parameterization of empirical forcefields for glassy silica using machine learning, MRS Commun. **9**, 593 (2019).

[53] H. Liu, Z. Fu, Y. Li, N. F. A. Sabri, and M. Bauchy, Balance between accuracy and simplicity in empirical forcefields for glass modeling: insights from machine learning, J. NonCryst. Solids **515**, 133 (2019).

[54] H. Liu, Y. Li, Z. Fu, K. Li, and M. Bauchy, Exploring the landscape of Buckingham potentials for silica by machine learning: soft vs hard interatomic forcefields, J. Chem. Phys. **152**, 051101 (2020).

[55] D. J. Evans and B. L. Holian, The Nose–Hoover thermostat, J. Chem. Phys. **83**, 4069 (1985).

[56] P. H. Hünenberger, Thermostat algorithms for molecular dynamics simulations, in *Advanced Computer Simulation: Approaches for Soft Matter Sciences I*, edited by C. Holm and K. Kremer (Springer, Berlin, Heidelberg, 2005), pp. 105–149.

[57] See Supplemental Material at http://link.aps.org/supplemental/10.1103/PhysRevB.106.214206 for more details about the simulations and the classification model.

[58] S. Plimpton, Fast parallel algorithms for short-range molecular dynamics, J. Comput. Phys. **117**, 1 (1995).

[59] A. Stukowski, Visualization and analysis of atomistic simulation data with OVITO–the open visualization tool, Modelling Simul. Mater. Sci. Eng. **18**, 015012 (2010).

[60] F. Pedregosa, A. Gramfort, V. Michel, B. Thirion, O. Grisel, M. Blondel, P. Prettenhofer, R. Weiss, V. Dubourg *et al.*, Scikit-learn: machine learning in Python, J. Mach. Learn. Res. **12**, 2825 (2011).

[61] R. Batuwita and V. Palade, Class imbalance learning methods for support vector machines, in *Imbalanced Learning*, edited by H. He and Y. Ma (John Wiley & Sons, Inc., Hoboken, 2013), pp. 83–99.

[62] S. Ispas, M. Benoit, P. Jund, and R. Jullien, Structural properties of glassy and liquid sodium tetrasilicate: comparison between *ab initio* and classical molecular dynamics simulations, J. NonCryst. Solids **307–310**, 946 (2002).

[63] C. M. Bishop, *Pattern Recognition and Machine Learning* (Springer, New York, 2006).

[64] L. Tang, G. Ma, H. Liu, W. Zhou, and M. Bauchy, Bulk metallic glasses' response to oscillatory stress is governed by the topography of the energy landscape, J. Phys. Chem. B **124**, 11294 (2020).

[65] L. Tang, H. Liu, G. Ma, T. Du, N. Mousseau, W. Zhou, and M. Bauchy, The energy landscape governs ductility in disordered materials, Mater. Horiz. **8**, 1242 (2021).

[66] A. Nicolas, E. E. Ferrero, K. Martens, and J.-L. Barrat, Deformation and flow of amorphous solids: insights from elastoplastic models, Rev. Mod. Phys. **90**, 045006 (2018).

[67] S. R. Elliott and F. E. G. Henn, Application of the anderson-stuart model to the ac conduction of ionically conducting materials, J. NonCryst. Solids **116**, 179 (1990).

[68] R. Freitas and E. J. Reed, Uncovering the effects of interface-induced ordering of liquid on crystal growth using machine learning, Nat. Commun. **11**, 3260 (2020).

[69] A. P. Bartók, R. Kondor, and G. Csányi, On representing chemical environments, Phys. Rev. B **87**, 184115 (2013); **87**, 219902(E) (2013); **96**, 019902 (2017).

[70] L. Himanen, M. O. J. Jäger, E. V. Morooka, F. Federici Canova, Y. S. Ranawat, D. Z. Gao, P. Rinke, and A. S. Foster, DScribe: library of descriptors for machine learning in materials science, Comput. Phys. Commun. **247**, 106949 (2020).